42nd AIAA Aerospace Sciences Meeting and Exhibit
5 - 8 January 2004, Reno, Nevada

AIAA 2004-641

EFFECTS OF FLOW PROPERTIES ON SOOT FORMATION AND OXIDATION RATES IN FLAME ENVIRONMENTS

C.H. Kim*, A.M. El-Leathy† and G.M. Faeth‡
The University of Michigan
Ann Arbor, Michigan 48109-2140

F. Xu**
The University of Central Florida
Orlando, Florida 32816-2450

ABSTRACT

Soot and flame structure were measured in a variety of round laminar premixed and nonpremixed (diffusion) jet flames fueled with hydrocarbons to study the properties of soot formation (primary soot particle nucleation and surface growth) and surface oxidation. The following properties were measured along the axes of the flames: soot concentrations by laser extinction, soot temperatures by multiline emission, soot structure by thermophoretic sampling and electron microscopy, concentrations of major gas species by sampling and gas chromatography, concentrations of some radical species (H, OH and O) by atomic absorption and flow velocities by laser velocimetry. These measurements were analyzed to yield local primary soot particle surface growth and surface oxidation rates, as well as primary soot particle nucleation rates. It was found that local soot surface growth rates could be correlated effectively using Hydrogen-Abstraction/Carbon-Addition (HACA) soot surface growth rate mechanisms in the literature; that local soot surface oxidation rates could be correlated effectively using OH/O_2 mechanisms in the literature; and that local soot particle nucleation rates (observable using electron microscopy techniques) could be correlated by assuming that the rate of development of large PAH molecules by the HACA mechanism controlled nucleation rates. These results were found considering a broad range of conditions in laminar flame environments: premixed and diffusion flames, various hydrocarbon fuel types (methane, acetylene, ethylene, propylene, propane and benzene), gas temperatures of 1500-2350 K and pressures of 10-100 kPa.

NOMENCLATURE

C_i = mass of carbon removed per mole of species i (kg kgmol^{-1})
d = fuel port exit diameter (m)
d_p = mean primary soot particle diameter (m)
f_s = soot volume fraction (-)
[i] = molar concentration of species i (kgmol m^{-3})
k = Boltzmann constant (J K^{-1})
k_H = constant in simplified soot surface growth rate formulation (kg m^4 kgmol^{-2} s^{-1})
k_n = primary soot particle nucleation rate constant (kgmol^{-n} m^{3n} s^{-1})
m_i = mass of a molecule of species i (kg molecule^{-1})
M_i = molecular weight of species i (kg kgmol^{-1})
n = order of the nucleation rate with respect to [H](-)
n_p = number of primary soot particles per unit volume (m^{-3})
Re = burner exit Reynolds number, $u_o d/\nu_o$
R_i = terms in HACA soot surface growth rate formulas (kg m^{-2} s^{-1})
R_u = universal gas constant (J kgmol^{-1} K^{-1})

* Graduate Student Research Assistant, Department of Aerospace Engineering.
† Research Fellow, Department of Aerospace Engineering.
‡ A.B. Modine Professor, Department of Aerospace Engineering; Fellow, AIAA; Corresponding Author, Tel.: +1-734-764-7202, Fax: +1-734-936-0106, E-mail address: gmfaeth@umich.edu
** Assistant Professor, Department of Mechanical, Materials and Aerospace Engineering.

S = soot surface area per unit volume (m^{-1})
t = time (s)
T = temperature (K)
u = streamwise velocity ($m\ s^{-1}$)
$\overline{v_i}$ = mean molecular velocity of species i, ($m\ s^{-1}$)
w_g = soot surface growth rate ($kg\ m^{-2}\ s^{-1}$)
w_{ox} = soot surface oxidation rate ($kg\ m^{-2}\ s^{-1}$)
z = streamwise distance (m)
α_i = empirical (steric) factors in HACA soot surface oxidation (-)
η_i = collision efficiency of species i for soot surface oxidation (-)
ν = kinematic viscosity ($m^2\ s^{-1}$)
ρ = gas density ($kg\ m^{-3}$)
ρ_s = soot density ($kg\ m^{-3}$)
ϕ = fuel-equivalence ratio (-)

Subscripts

CH = HACA soot surface growth mechanism of Colket and Hall[18]
FW = HACA soot surface growth mechanism of Frenklach and coworkers[19-21]
o = burner exit condition

INTRODUCTION

The presence of soot is a common feature of nonpremixed (diffusion) flames fueled by hydrocarbons, influencing their structure, transport and chemical reaction properties. As a result, soot processes in flames affect capabilities for computational combustion due to the complexities of soot chemistry, public health due to emissions of pollutant particulate soot, fire safety due to increased fire growth and spread rates caused by soot radiation, and combustor durability due to heat loads caused by continuum radiation from soot. Motivated by these observations, the present investigation sought to extend past work on soot surface growth and surface oxidation in laminar premixed and diffusion flames in this laboratory, see Refs. 1-9, seeking to broaden the range of temperatures and pressures in flames considered for measurements of soot surface reaction properties from past work, and to undertake initial considerations of primary soot particle nucleation properties in flame environments. The present description of the investigation is relatively brief, see Kim et al.[10] and El-Leathy et al.[11] for more details.

Early studies of the structure and reaction properties of soot in flame environments have been reviewed by Haynes and Wagner,[12] Howard,[13] Richter and Howard[14] and Kennedy;[15] therefore, the following discussion of these properties will be brief and will emphasize past studies in this laboratory that have motivated the objectives and developed the methods of the present investigation. Sunderland and coworkers[1-3] experimentally studied the structure and soot surface growth properties of laminar hydrocarbon-fueled (acetylene, ethylene, propane, n-butane, propylene, and 1,3 butadiene) diffusion flames burning in air at pressures of 0.1-1.0 atm; unfortunately, they were not able to evaluate mechanisms of soot surface reactions because their measurements did not provide information about radical concentrations (H, OH and O) needed by existing theories of these processes. Xu and coworkers[4-6] subsequently completed experimental investigations of the structure and soot surface growth properties of laminar premixed flames at atmospheric pressure including ethylene/air mixtures similar to the flames studied by Harris and Weiner[16] and methane/oxygen mixtures similar to the flames studied by Ramer et al.[17] Concentrations of H were found during these studies; therefore, these measurements could be used to evaluate the Hydrogen-Abstraction/Carbon-Addition (HACA) soot surface growth mechanisms of Colket and Hall[18] and Frenklach and coworkers.[19-21] It was found that these HACA soot surface growth mechanisms provided excellent correlations of the measurements using quite reasonable values of the unknown empirical steric factors that appear in the theories. Xu and Faeth[7] and El-Leathy et al.,[8] extended the study of soot surface growth from premixed flames to laminar jet diffusion flames fueled with a variety of hydrocarbons (acetylene, ethylene, propylene, propane and benzene) burning in air at atmospheric pressure. These measurements showed that soot surface growth rates in laminar premixed and diffusion flames satisfied similar reaction rate expressions, that effects of hydrocarbon fuel type on soot surface growth rates were small, and that soot surface growth rates were well represented by the HACA mechanisms of Colket and Hall[18] and Frenklach and coworkers.[19-21] Continuing questions about soot surface growth in flames, however, involve behavior at pressures other than atmospheric pressure and at temperatures of interest for practical applications but greater than those considered in Refs. 4-8, e.g., greater than 2000 K.

Soot surface oxidation was also considered during the studies of soot reaction properties in diffusion flames at atmospheric pressure of Xu and coworkers and are reported in Xu et al.[9] They established that soot surface oxidation at fuel-rich and near-stoichiometric conditions, involving a variety of hydrocarbon fuels (acetylene, ethylene, propylene, propane and benzene), was dominated by reaction of the soot surface with OH, and could be correlated effectively by estimating the oxidation rate due to direct

attack by O_2 using the classical expression of Nagle and Strickland-Constable[22] (which was later confirmed by Park and Appleton[23]), combined with an oxidation rate due to OH that had very nearly the same collision efficiency as the results of Neoh and coworkers,[24,25] based on measurements in soot-containing premixed flames at atmospheric pressure. This finding is also in fair agreement with earlier measurements of soot surface oxidation rates by OH in diffusion flames at atmospheric pressure due to Garo et al.[26,27] and Hardiquert et al.[28] Similar to the findings for soot surface growth, however, past determinations of soot surface oxidation properties have been limited to atmospheric pressure and temperatures less than 2000 K.

The properties of soot structure (observable using visible light and electron microscopy techniques) needed to help define primary soot particle nucleation properties have attracted considerable attention, see Heckman and Harling,[29] Wersborg et al.,[30] Lahaye and Prado,[31] Hess and Herd,[32] Köylü and Faeth,[33] Köylü et al.,[34] Ishiguro et al.,[35] Dobbins,[36] Chen and Dobbins,[37] and references cited therein. Based on these investigations, it is generally agreed that soot particles consist of nearly spherical and monodisperse primary soot particles (standard deviations of primary soot particles generally are less than 10%) at a given flame condition, that these primary soot particles are collected into Hausdorf or mass fractal aggregates, and that these aggregates exhibit large variations in the number of primary soot particles per aggregate at a given flame condition (generally best represented by a log normal probability density distribution). These properties are illustrated by the Transmission Electron Microscope (TEM) photograph of soot aggregates observed at a typical flame condition during the present investigation that appears in Fig. 1. These studies have also shown that the inner structure of TEM-observable primary soot particles consists of two regions: (1) an inner core, often taken to represent a primary soot particle at the completion of nucleation, made up of several smaller (or fine) particles having an irregular structure that have coalesced to form the nucleus, and (2) an outer shell-like region that results from the systematic addition of carbon to the primary soot particle by the surface growth mechanism.[31,32,35-37] Other studies have considered the formation of soot precursor species that eventually coalesce to form the fine particle portions of primary soot particles. These particles are only observable using ultra-violet light absorption and scattering or Scanning Mobility Particle Sizer (SMPS) techniques to observe particles having diameters as small as 3 nm, see Dobbins et al.,[38,39] D'Alessio et al.,[40] Zhao et al.,[41,42] and references cited therein. In particular, Zhao et al.,[41,42] observed decreasing numbers of these fine particles as their diameters increase in the range 3-10 nm, suggesting coalescence of the fine particles to form TEM-observable primary soot particle nuclei that typically have diameters on the order of 10 nm. Finally, Roesler et al.,[43] and references cited therein, suggest that these fine particles form by coalescence of precursor species consisting of large Polyatomic Aromatic Hydrocarbon (PAH) molecules, and that these PAH species that tend to be relatively stable at high temperatures, called stabilomers by Stein and Fahr.[44] In turn, these PAH species are thought to grow according to HACA mechanisms, similar to the mechanism of soot surface growth that yields the outer shell structure of primary soot particles. In fact, an analogy between PAH growth and primary soot particle surface growth was adopted when the HACA mechanism was initially proposed as the mechanism of primary soot particle surface growth, see Frenklach and Wang.[19] These studies, however, have not yet developed a method for estimating the rate of nucleation of TEM-observable primary soot particles needed to exploit the primary soot particle surface growth and surface oxidation results of Xu and coworkers[4-9]

To summarize, recent work considering primary soot particle surface growth and oxidation properties has provided a start toward achieving capabilities to estimate the properties of soot in flame environments but information about primary soot particle surface growth and surface oxidation properties is needed at pressures other than atmospheric pressure and at temperatures greater than 2000 K; in addition, more must be known about the nucleation properties of the TEM-observable primary soot particles that initiate soot surface growth and oxidation processes after they are formed. Thus, the objectives of the present investigation were as follows:

1. To complete new measurements of primary soot particle surface growth and oxidation properties at pressures of 0.1-1.0 atm and at temperatures greater than 2000 K and to use these measurements to evaluate the capabilities of existing HACA mechanisms of soot surface growth and OH/O_2 mechanisms of soot surface oxidation to correctly treat effects of variable pressure and high temperature soot-containing environments.

2. To exploit available information about the nucleation rates of TEM-observable primary soot particle nucleation rates to develop an approximate method to estimate primary soot particle nucleation properties so that the combined methodology

provides a way to estimate soot properties in flame environments.

EXPERIMENTAL METHODS

Premixed Flame Apparatus

The same experimental apparatus was used for both of the present studies of the soot formation and surface oxidation in laminar premixed flames.[4,5] The premixed flames were produced by a 60 mm diameter water-cooled porous-plate laminar flat flame burner directed vertically upward at atmospheric pressure. The reactant mixture was surrounded by a 6 mm wide annular nitrogen coflow to eliminate the peripheral diffusion flames that are present when fuel-rich premixed flames are burned in room air. The flames were stabilized by impinging the burner flow on a flat plate having a 30 mm diameter hole centered on the flame axis, 32 mm above the burner exit. The flames were surrounded by layers of screens and a plastic enclosure in order to avoid room disturbances. The burner could be traversed in the horizontal and vertical directions in order to accommodate rigidly-mounted optical instruments.

Diffusion Flame Apparatus

Two different test arrangements were used to study soot properties in laminar diffusion flames: one for studies at atmospheric pressure, and one for studies at pressures of 0.1-1.0 atm. The atmospheric pressure burner is described by Xu and Faeth,[7] it involved a 34.8 mm diameter port for the fuel stream and a 60 mm diameter coannular outer port for the oxidizer stream, both directed vertically upward. These flames were surrounded by layers of screens and a plastic enclosure to avoid room disturbances. This burner could be traversed in the horizontal and vertical directions in order to accommodate rigidly-mounted optical instruments.

The variable-pressure burner is described by Kim et al.,[10] it involved a 3.3 mm diameter port for the fuel stream, directed vertically upward. The flames burned along the axis of a vertical windowed chamber having a diameter and length of 300 mm. The top and bottom of the chamber consisted of porous plates that separated the flame chambers from plenum chambers for air inflow and exhaust outflow and provided a uniform distribution of air flow over the chamber cross section. The entire test chamber could be traversed in the vertical and horizontal directions in order to accommodate rigidly-mounted optical instruments.

Instrumentation

Measurements in the premixed and diffusion flames were limited to the axes of the flames and were similar for all the flames to be considered, e.g., Refs. 4-11, as follows:

Soot volume fractions were measured by deconvoluting laser extinction measurements at a visible wavelength of 632.8 nm for chord-like paths through the flames. This data was reduced using the refractive indices of Dalzell and Sarofim[45] in order to be consistent with past work,[1-11] however, these values have recently been confirmed by Krishnan et al.[46,47] The experimental uncertainties (95% confidence) of the measured soot volume fractions are estimated to be smaller than 10% for soot volume fractions greater than 0.02 ppm, increasing inversely proportional to the soot volume fraction for smaller values.

Primary soot particles are small (smaller than 50 nm diameter); therefore, soot and gas temperatures are essentially the same. Thus, soot (gas) temperatures were measured by deconvoluting spectral radiation intensities for continuum radiation from soot for chord-like paths through the flames and computing temperatures at seven wavelength pairs in the wavelength range of 550-830 nm. Temperature differences between the average and any of the individual line pairs were less than 50-100 K and experimental uncertainties (95% confidence) of these measurements were less than 50 K. This level of accuracy was adequate because primary soot particle surface reaction and nucleation rates were relatively insensitive to direct effects of temperature.

Concentrations of major gas species (N_2, Ar, H_2O, O_2, CO, CO_2, CH_4, C_2H_4, C_2H_6, C_3H_6, and Ne (the last being a tracer gas used to estimate effects of radial diffusion of lithium-containing species that was used to find H, OH and O concentrations) were measured by isokinetic sampling (based on flow velocity measurements to be discussed later) and analysis by gas chromatography. Experimental uncertainties (95% confidence) of these measurements were mainly due to calibration uncertainties and are estimated to be less than 5% for all species concentrations reported here. Finally, present limits of detection for all these species were all smaller than 20 ppm at atmospheric pressure ranging up to 200 ppm at 0.1 atm, the lowest pressure tested.

Soot structure measurements were carried out by thermophoretic sampling and either TEM or HRTEM. Primary soot particles were nearly spherical and monodisperse at given positions in each flame

(standard deviations of primary soot particle diameters were less than 10%) and experimental uncertainties (95% confidence) of soot primary particle measurements are estimated to be less than 10%.

Streamwise gas velocities were measured using laser velocimetry based on seeding the flame gases with aluminum oxide particles having nominal diameters of 1000 nm, similar to past work.[1-11] The experimental uncertainties (95% confidence) of these measurements were less than 5%, largely based on calibration uncertainties.

Measurements of the concentrations of H, OH and O were carried out using deconvoluted absorption in the visible for chord-like paths through the flames following the Li/LiOH atomic absorption technique of Neoh et al.[24,25] The correction for the radial diffusion of the LiOH seed (and its dissociation products) used for these measurements was found from the measurements of Ne seed placed in the flow, assuming that the mass diffusivities of the lithium-containing species and Ne were similar. The determination of H concentrations was calibrated using a premixed flame, as discussed by Xu and Faeth,[6] again following Neoh et al.[24,25] Measurements using different initial concentrations of Li/OH seed showed that the effects of this seed on flame properties were negligible. Experimental uncertainties (95% confidence) of the H concentration measurements are estimated to be smaller than 30%. Given the concentrations of H, O_2, H_2 and H_2O in the flow, the concentrations of OH and O were computed assuming partial equilibrium among these radical species and corresponding stable species, following Neoh et al.[24,25] and using the equilibrium constant data of Chase et al.[48] The experimental uncertainties of OH and O concentrations were comparable to those of H. Finally, the limits of detection of H, OH and O were all smaller than 0.01 ppm.

SOOT REACTION PROPERTIES

The measurements obtained from the laminar premixed and diffusion flames were used to find primary soot particle nucleation and surface growth and oxidation rates. Major assumptions were identical to earlier work,[1-11] as follows: soot surface growth, rather than soot nucleation, dominates soot mass production; soot surface oxidation dominates soot oxidation; soot nucleation is limited to consideration of TEM-observable primary soot particles upon which soot surface reaction processes subsequently occur; effects of diffusion (Brownian motion) and thermophoresis on soot particle motion are small, so that soot particles convect along the axes of the flames at the local gas velocity; the soot density is a constant, adopting the value of 1850 kg/m^3 similar to past work;[1-11] and the surface available for soot surface growth and oxidation is equivalent to constant diameter spherical primary soot particles that meet at a point, see Refs. 1-11 for justification of these assumptions.

The first primary soot property of interest is the number of primary soot particles per unit volume. This property was found from the measurements of soot volume fractions and primary soot particle diameters, as follows:[1]

$$n_p = 6f_s/(\pi d_p^3) \quad (1)$$

The experimental uncertainties (95% confidence) of n_p are estimated to be less than 32% for $f_s > 0.1$ ppm, increasing inversely proportional to f_s for values smaller than 0.1 ppm. The soot surface area per unit volume is given by the same measurements, as follows:[1]

$$S = 6f_s/d_p \quad (2)$$

The experimental uncertainties (95% confidence) of S are estimated to be less than 16% for $f_s > 0.1$ ppm, increasing inversely proportional to f_s for smaller values of f_s.

The primary soot particle nucleation rate was defined as the rate of increase of the number of primary soot particles per unit volume and time. Then based on the previous assumptions, the expression for the primary soot particle nucleation rate for motion along a streamline at the axis of the test flames becomes:

$$w_n = \rho\, d(n_p/\rho)/dt \quad (3)$$

where n_p found from Eq. 1 and the gas density in Eq. 3 was found from measurements of gas species concentrations and temperatures, assuming an ideal gas mixture and neglecting the volume of soot (which was only present at ppm levels throughout the present data base). The temporal derivative in Eq. 3 was converted into a spatial derivative (which better suited present measurements) based on the convection approximation, as follows:

$$d(\,)/dt = u\,d(\,)/dz \quad (4)$$

The spatial derivative of Eq. 4, needed to compute w_n, was found from three-point least squares fits of the argument of the derivative, n_p/ρ, similar to past work.[1-11] The resulting experimental uncertainties (95%

confidence) of w_n were rather large (50%), due to the amplification of experimental uncertainties when the spatial derivative in Eq. 4 was found.

Primary soot particle surface growth rate was defined as the rate of increase of soot mass per unit soot surface area and time; whereas, the soot surface oxidation rate was defined as the rate of decrease of soot mass per unit surface area and time. Then, based on the previous assumptions, the expressions for the primary soot particle surface growth and oxidation rates, for motion along a streamline at the axis of the test flames, becomes:

$$w_g = -w_{ox} = (\rho/S)d(\rho_s f_s/\rho)dt \qquad (5)$$

where present measurements of species concentrations and temperatures yield the gas density, assuming an ideal gas mixture, and a minus sign is inserted in Eq. 5 so that w_{ox} is a positive number. Similar to the determination of w_n, the temporal derivatives in Eq. 5 were converted into a spatial derivative using Eq. 4. Finally, consideration of soot surface oxidation was limited to early soot surface oxidation (soot mass consumption less than 70%) where problems of soot aggregate breakup, the development of primary soot particle porosity, and the internal oxidation of primary soot particles, do not yet occur, see Neoh et al.[25] Estimated experimental uncertainties (95% confidence) of soot surface reaction rates are less than 30%.

TEST CONDITIONS

The properties of the test flames are briefly summarized in Table 1; they include six (6) premixed flames studied by Xu et al.[4,5] and sixteen (16) diffusion flames studied by Xu and coworkers.[7-11] The premixed flames consisted of the ethylene/air and methane/oxygen flames at atmospheric pressure considered by Harris and Weiner[16] and Ramer et al.[17] The diffusion flames were fueled with a variety of hydrocarbons (acetylene, ethylene, propylene, propane and benzene) burning either air or O_2/Ar mixtures at pressures of 0.1-1.0 atm. Finally, acetone contamination of acetylene, a potential difficulty pointed out by Hamins et al.[49] and Colket et al.[50,51] is not thought to be a problem for the present measurements based on evaluation of this effect by Xu and Faeth,[7] for acetylene/air laminar jet diffusion flames at atmospheric pressure.

RESULTS AND DISCUSSION

Soot Structure

The soot particles observed during the present investigation were similar to those seen during earlier studies in laminar premixed and diffusion flames.[33-39] A TEM photograph of soot particles observed at a typical flame condition during the present investigation appears in Fig. 1. In agreement with earlier observations, Refs. 33-39, the present soot particles consist of nearly spherical and monodisperse primary soot particles (standard deviations of primary soot particle diameter were less than 10%) at each flame condition, that these primary soot particles were collected into Hausdorf or mass fractal aggregates, and that these aggregates exhibited large variations of the number of primary soot particles per aggregate at a given flame condition (generally best represented by a log normal probability density distribution).

More magnified images of the present soot aggregates appear in Fig. 2, which shows TEM (left image with a 50 nm length scale) and HRTEM (right image with a 10 nm length scale). These photographs were obtained at the maximum soot volume fraction location along the axis of a C_2H_2-Ar/O_2-Ar diffusion flame at atmospheric pressure. TEM and HRTEM images of soot particles at other flame conditions considered here, however, were qualitatively similar. In general, the primary soot particles exhibited an outer shell having a sheetlike structure parallel to the outer surface of the primary soot particles, and an irregular inner core that appears to result from the coalescence of several smaller primary soot particles near the soot nucleation condition, as described by Ishiguro et al.,[35] Dobbins,[36] and Chen and Dobbins.[37] The less sheetlike and more irregular nature of the inner core of the primary soot particles for present conditions was most evident from HRTEM images obtained near the end of soot oxidation, where the outer shell has largely been oxidized away, see El-Leathy et al.[8] for HRTEM images at this condition.

Finally, all primary particles observed during the present studies exhibited identical soot surface reaction properties. Furthermore, HRTEM images of these primary soot particles indicated that they consisted of amorphous soot with no evidence of graphitic structures within them, similar to the HRTEM image appearing in Fig. 2. This behavior is typical of past observations of the structure of primary soot particles in flame environments, see Refs. 31 and 35-37 and references cited therein.

Premixed Flame Structure

Measurements of the structure of a typical soot-containing laminar premixed flame considered during the present investigation are illustrated in Fig. 3. This flame is a premixed ethylene/air flame at atmospheric pressure with the reactant stream having concentrations of 15.6% C_2H_2 and 84.4% air, by volume, obtained from the measurements of Xu et al.[4] Results for other premixed flames considered by Xu et al.,[4,5] however, were qualitatively similar. Flame structure properties appearing in the figure include temperatures, velocities, soot volume fractions, primary soot particle diameters, the concentrations of major gas species and the concentration of the radial species H. An example of the reactive properties of this flame is provided by plots of the number of primary soot particles per unit volume and the rate of formation of primary soot particles, corresponding plots of soot surface area per unit volume and soot surface growth rates can be found in Xu et al.[4,5] Elapsed residence times in the flame (relative to the first position where finite soot volume fractions were observed) appear at the top of the plot.

Effects of buoyancy were significant for the flame conditions of Fig. 3; therefore, streamwise velocities increase from small burner exit values to 1000 mm/s at z=30 mm. The presence of continuum radiation heat losses from soot cause temperatures to decrease from roughly 2000 K (at z=7 mm) to roughly 1500 K at z=28 mm. Finite soot volume fractions are first observed near z=7.5 mm, subsequently, soot volume fractions increase for a time and then level off with increasing distance from the burner exit which is a well known trend for soot-containing laminar premixed flames, see Haynes and Wagner,[12] Harris and Weiner[16] and Ramer et al.[17] The range of primary soot particle diameter measurements corresponds to conditions where soot volume fractions could be measured with acceptable experimental uncertainties, which involves mean primary particle diameters larger than 10 nm. For the range of measurements illustrated in Fig. 3, mean primary particle diameters increase for a time and then level off with increasing distance from the burner exit, similar to the behavior of soot volume fractions. The concentrations of major stable gas species agree with earlier observations of Harris and Weiner;[16] they are nearly constant throughout the soot formation region which suggests that rates of soot formation in premixed flames do not decrease due to consumption of soot-forming hydrocarbon species, e.g., CH_4, C_2H_4 and C_2H_2. In contrast, rates of soot formation are seen to progressively decrease proportional to the decrease of the concentration of the radical species H, with increasing distance from the burner exit. Noting that rates of soot surface growth, that dominate rates of soot formation, are proportional to the concentration of H as a first approximation of the HACA mechanisms of soot surface growth,[18-21] this behavior supports the hypothesis that soot surface growth in premixed flames is dominated the HACA mechanism. Xu and coworkers[4-6] also showed that concentrations of H in the slowly developing post-flame region of premixed soot-containing flames approximate thermodynamic equilibrium very closely. Thus, the reduction of H concentrations with increasing streamwise distance in Fig. 3 is a direct result of the reduction of temperature which reduces the equilibrium constant proportional to the yield of H. Thus, radiative heat losses from soot actually tend to reduce the rate of formation of soot in premixed flames.

Turning to the nucleation properties of primary soot particles observable using electron microscopy methods, the number of primary soot particles per cubic meter is seen to increase with increasing distance from the burner exit and then level off in Fig. 3, behaving similar to the variation of f_s with distance from the burner exit. Similarly, the rate of formation of primary soot particles per unit volume is largest near the region where soot formation is first observed and then progressively decreases as a function of distance from the burner exit. This behavior is qualitatively similar to the variation of the concentration of the radical species, H, as a function of distance from the burner exit. This suggests that soot particle nucleation rates are controlled by a mechanism somewhat similar to soot surface growth rates, e.g., the HACA mechanism of soot surface growth. Such behavior is not surprising, however, because the formation and growth of PAH species that are thought to eventually coalesce to form a soot nucleus proceeds by the HACA mechanism.

Diffusion Flame Structure

Measurements of the structure of a typical soot-containing laminar diffusion flame are illustrated in Fig. 4. This flame involves an ethylene-fueled laminar jet diffusion flame burning in coflowing air at atmospheric pressure, however, results for other diffusion flames considered by Xu and coworkers[7-11] are qualitatively similar. Flame structure properties appearing in the figure include temperatures, velocities, soot volume fractions, primary soot particle diameters, the concentrations of major gas species, the concentrations of some radical species (H, OH and O), the number of primary particles per unit volume and the rate of formation of primary particles per unit volume. These properties are plotted for conditions along the axis of the flame, as a function of height above the burner exit. Elapsed residence times in the flame (relative to the first position where finite soot

volume fractions were observed) appear at the top of the plot. The right hand boundary of Fig. 4 represents the limit of yellow soot luminosity although soot concentrations were too small to be measured accurately as this limit was approached. The flame sheet location, where ϕ=1 is also marked on the plot indicating that soot oxidation extends into the fuel-lean region of the flame. This is not always the case, however, and flames where both soot formation and oxidation were completed at fuel-rich conditions were also observed.

Gas velocities increase from small burner exit conditions to values in excess of 2000 mm/s for the ethylene-fueled flame of Fig. 4, indicating significant effects of buoyancy for this flame, typical of most diffusion flames studied by Xu and coworkers[7-11] Gas temperatures reach a weak maximum well below the adiabatic flame temperature for these reactants, due to radiative heat losses which is quite significant for soot-containing flames. Unlike premixed flames, e.g., Fig. 3, primary soot particle diameters in diffusion flames reach maximum values relatively early in the soot formation region as seen in Fig. 4. This behavior is caused by the fact that soot nucleation rates tend to accelerate with increasing distance in the soot formation region at conditions prior to reaching the maximum primary particle diameter in diffusion flames whereas this rate progressively decreases with increasing distance in the soot formation region in premixed flames. This behavior causes the relatively few soot particles formed near soot inception conditions for diffusion flames, that become large due to lengthy residence times for soot surface growth, to be superseded by large numbers of primary soot particles created later in the soot formation period, that are smaller due to smaller residence times for soot surface growth. Notably, Tesner[52,53] has observed that soot surface growth remains rapid at soot inception conditions in diffusion flames where soot nucleation rates are small, which is consistent with the present observations. For acetylene-fueled flames, acetylene concentrations progressively decrease with increasing distance within the soot-containing region. This behavior extends to other fuels, such as ethylene in Fig. 4, because the original fuel disappears relatively early in the soot formation region to yield hydrogen and hydrocarbon species that are relatively robust in high-temperature flame environments, particularly acetylene which is a relatively stable fuel compound at high temperatures. In addition, acetylene is especially important as a fuel decomposition product because it is a major building block of PAH which feeds primary soot particle nucleation, and it also is a major reactant for the HACA soot surface growth mechanism.[18-21] In addition to fuel species important for the formation of soot, the soot formation region also contains significant concentrations of species potentially capable of soot oxidation (e.g., O_2, CO_2, H_2O, OH and O). Thus, soot formation and oxidation occur at the same time in diffusion flames with the soot formation region (the region before the maximum soot volume fraction condition is reached) involving conditions where primary soot particle nucleation and surface growth are more important than soot surface oxidation whereas the soot oxidation region (the region after the maximum soot volume condition is reached) involves conditions where soot surface oxidation is more important than soot nucleation and surface growth. Finally, OH and O generally increase monotonically with increasing distance into the soot-containing region whereas concentrations of H reach a broad maximum just on the fuel-rich side of the flame sheet (the ϕ=1 condition).

Turning to the nucleation properties of primary soot particles, observable using electron microscopy methods, the maximum number of primary soot particles per unit volume is reached on the fuel-rich side of the flame sheet and roughly at the maximum soot volume fraction condition. In contrast, the maximum rate of production of primary soot particles per unit volume is reached in the region between the maximum primary soot particle diameter and the maximum soot volume conditions. This highlights the effect of the large increases in the number of primary soot particles in the flow or reducing the mean primary particle diameter.

Soot Surface Growth Rates

The gross soot surface growth rates for all flames considered here were corrected for effects of soot surface oxidation, using the mechanism of soot surface oxidation determined during the present study. In order to control experimental uncertainties, however, no soot surface growth measurements considered in the following involved a correction for soot surface oxidation that was larger than 50% of the gross soot surface growth rate.

Soot surface growth rates were interpreted using the HACA soot surface growth mechanisms of Colket and Hall[18] and Frenklach and coworkers[19-21] in order to be consistent with past work, e.g., Refs. 4-11. In all cases, net soot surface growth rates were expressed as follows:

$$w_g = \alpha_i R_i \qquad (6)$$

where i=CH or FW denotes reaction parameters for the HACA soot surface growth rate mechanisms of Colket

and Hall[18] and Frenklach and coworkers,[19-21] respectively. The parameters, α_i, are empirical steric factors on the order of unity, with α_{CH} specified to be a constant,[18] and α_{FW} specified to be a function of temperature.[19-21] The details of these mechanisms, the formulas for the R_i, and the reaction rate parameters used when computing the R_i, can be found in Xu et al.[4] An exception to the description of Xu et al.[4], however, was that the Colket and Hall[18] mechanism was modified based on the study of soot surface growth at pressures of 0.1-1.0 atm due to Kim et al.[10] In particular, Kim et al.[10] found that Reaction No. 3 of the mechanism of Colket and Hall,[18] e.g.,

$$C_s\bullet \rightarrow C_2H_2 + \text{products} \qquad \text{(R3)}$$

where $C_s\bullet$ represents a radical site on the surface of a primary soot particle, caused the Colket and Hall,[18] mechanism to yield a poor correlation of the measurements at small pressures. To correct this difficulty, Reaction No. 3 was deleted from the Colket and Hall,[18] mechanism, which results in a smaller best-fit value of α_{CH} than found during earlier work (e.g., Refs. 4-8) as discussed later. In contrast, the mechanism of Frenklach and coworkers,[19-21] and the correlation of α_{FW} as a function of temperature, were unchanged from earlier work, e.g., Refs. 4-8.

As a first approximation for all the flames considered here, the R_i are proportional to the product $[H][C_2H_2]$. Thus, in order to directly evaluate the HACA soot surface growth mechanism without the uncertainties associated with specific reaction mechanisms, values of $w_g/[C_2H_2]$ are plotted as a function of [H] in Fig. 5. The laminar flame measurements considered in Fig. 5 include the premixed flame measurements of Xu et al.,[4,5] and the diffusion flame measurements of Xu and Faeth,[7] El-Leathy et al.,[8,11] and Kim et al.[10] Taken together, these measurements involve premixed and diffusion flames, a variety of hydrocarbons (CH_4, C_2H_2, C_2H_4, C_3H_6, C_3H_8 and C_6H_6), pressures of 0.1-1.0 atm, and temperatures within the soot-containing regions of 1500-2350 K. An empirical correlation of the measurements is also illustrated in Fig. 5 as follows:

$$w_g = k_H[H][C_2H_2] \qquad (7)$$

where k_H = 2.85E+07 kg $m^4/(kgmol^2 s)$ with an experimental uncertainty (95% confidence) of 12%. This correlation is remarkably good and provides strong evidence that the HACA mechanism is responsible for soot surface growth.

A more direct evaluation of the HACA mechanism of soot surface growth is obtained by plotting w_g directly as a function of $\alpha_{CH}R_{CH}$ for the mechanism of Colket and Hall[18] (after finding the best-fit value of α_{CH}) as illustrated in Fig. 6. The measurements illustrated in Fig. 6 are the same as those considered in Fig. 5. The value of α_{CH} = 0.35 with an uncertainty (95% confidence) of 0.04. Finally, the mechanism of Frenklach and coworkers[19-21] is unaffected by pressure and yielded the following correlation for α_{FW}:

$$\alpha_{FW}(T) = 0.017 \exp(12100/T) \qquad (8)$$

with T(K) and the corresponding plot of w_g as a function of $\alpha_{FW}R_{FW}$ is qualitatively similar to the plot illustrated by Xu and Faeth.[7] This provides a satisfactory correlation of the HACA mechanism of Frenklach and coworkers[19-21] over the experimental range defined earlier, with values of α_{FW} on the order of unity and the negative activation energy implied by Eq. 8 corresponding to behavior anticipated by Frenklach and coworkers.[19-21]

Primary Soot Particle Nucleation Rates

Findings to date concerning the nucleation of transmission-electron-observable primary soot particles suggest a simplified approach to provide an approximate correlation of their nucleation rates. First of all, it is generally agreed that primary soot particle formation comes about by the formation of PAH species that coalesce to form a primary soot particle nucleus consisting of several PAH molecules, see Refs. 29,35 and 36. Next, it is generally agreed that PAH forms via the HACA mechanism; in fact, the basis of the HACA soot surface growth mechanisms of Colket and Hall[18] and Frenklach and coworkers[19-21] involved postulating similarities between PAH and soot surface growth. This idea is supported by the results illustrated in Figs. 3 and 4, noting that soot nucleation occurs wherever both H and acetylene are simultaneously present and ends when the concentration of either of these reactants becomes small, which is very similar to the behavior of the HACA soot surface growth mechanisms. Then assuming that the amount of time for the numerous collisions of H and C_2H_2 molecules with PAH molecules that is required to form large PAH molecules is much greater than the amount of time required for several PAH molecules to coalesce and dehydrogenate to form the nucleus of a primary soot particle, it seems reasonable to propose a simple HACA soot surface particle nucleation rate model as follows:

$$w_n = k_n[C_2H_2][H]^n \qquad (9)$$

where k_n is the primary soot particle nucleation rate constant and n is the molecular order of the primary soot particle rate expression with respect to the concentration of H.

Initial attempts to correlate primary soot particle nucleation rates along the lines of Eq. 9 indicated $w_n \sim [C_2H_2][H]^2$. Thus, in order to illustrate this correlation $w_n/[C_2H_2]$ is plotted as a function of $[H]^2$ in Fig. 7. Results illustrated in Fig. 7 include a variety of laminar flames: measurements of Xu and coworkers[4,5] in premixed flames and measurements of Xu and coworkers[7-11] in diffusion flames. In addition to the individual measurements, the best-fit correlation of the measurements according to Eq. 9 is illustrated on the plot. The formula for this correlation is as follows:

$$w_n = 2.6E{+}08[C_2H_2][H]^2 \qquad (10)$$

where w_n (kgmol primary particles/m^{3}s) and [i] (kgmol of i/m^3). The range of flame conditions considered in Fig. 7 is as follows: premixed and diffusion flames, various hydrocarbon fuels (methane, ethylene, propylene, propane and benzene), concentrations of acetylene of 8E-05 to 6E-02 kgmol/m^3, concentrations of H of 3E-08 to 3E-06 kgmol/m^3, temperatures of 1500-2350 K, and pressures of 0.1-1.0. Improvement of Eq. 10 was sought by considering k_n to be a function of temperature, however, this yielded a scattered correlation for k_n and no significant improvement of the correlation for w_n and is not reported here. The scatter of w_n in Fig. 7 is appreciable and is no doubt due to the simplified and incomplete nature of the present HACA-mechanism-dominated primary soot particle nucleation rate model. Contributing factors, however, are the relatively large experimental uncertainties (95% confidence) of n_p of 32% and of w_n of 50% to yield final experimental uncertainties (95% confidence) of the fit of the correlation of Eq. 10 of 43%.

Soot Surface Oxidation Rates

Present measurements of soot surface oxidation rates were corrected for effects of soot surface growth rates based on the Colket and Hall[18] soot surface growth rate mechanism as discussed in connection with Fig. 6. No condition is considered in the following, however, where the correction for effects of soot surface growth was more than half the gross soot surface oxidation rate. In addition, no condition was considered where more than 70% of the maximum soot mass had been oxidized. This was done to avoid the complications of porous soot surfaces and internal oxidation of primary soot particles observed by Neoh et al.[25] toward the last stages of soot primary particle oxidation.

Soot surface oxidation rates (corrected for soot surface growth) were converted into collision efficiencies based on kinetic theory estimates of the collision rates of a given gas species with the surface of primary soot particles, following Neoh et al.[24]:

$$\eta_i = 4w_{ox}/(C_i[i]\,\bar{v}_i) \qquad (11)$$

where C_i is the mass of carbon removed from the surface per mole of species i reacting at the surface, [i] is the gas phase concentration of i (kgmol/m^3) adjacent to the surface, and

$$\bar{v}_i = (8R_uT/(\pi M_i))^{1/2} \qquad (12)$$

is the Boltzmann equilibrium mean molecular velocity of species i. Values of η_i were measured for several species potentially responsible for soot surface oxidation, considering i = O_2, CO_2, H_2O and OH.

Collision efficiencies of O_2 for soot surface oxidation are plotted as a function of height above the burner in Fig. 8. Results shown in this and the next figure are as follows: values observed for premixed flames at atmospheric pressure by Neoh et al.,[24] values observed for diffusion flames fueled with a variety of hydrocarbons at atmospheric pressure due to Xu et al.,[9] and El-Leathy et al.,[11] values observed for acetylene-fueled flames at pressures of 0.1-1.0 due to Kim et al.,[7] and values estimated from the predictions of the Nagle and Strickland-Constable[22] correlation for conditions within the diffusion flames. The Nagle and Strickland-Constable[22] correlation is widely recognized to be effective for estimating soot surface oxidation rates due to O_2, and there are significant concentrations (0.1-10% by volume) of O_2 along the soot paths of many of the flames considered in Fig. 8, see Refs. 6-10. Thus, the fact that the Nagle and Strickland-Constable[22] estimates of O_2 collision efficiencies are 10-100 times smaller than the measurements in diffusion flames suggests that some other species is responsible for soot surface oxidation in flames. The large scatter of the O_2 collision efficiencies in Fig. 8 in both premixed and diffusion flames supports this conclusion. Results for CO_2, H_2O and O yielded similar conclusions to the O_2 results just discussed.

Finally, the collision efficiencies of OH for soot surface oxidation are plotted as a function of height above the burner in Fig. 9. With a few exceptions, at low temperature conditions toward the end of soot oxidation (where the development of primary particle porosity and internal oxidation might be a factor),

direct O_2 surface oxidation of soot is not very important for the flames considered in Fig. 9, similar to the results illustrated in Fig. 8. On the other hand, collision efficiencies for OH in the present diffusion flames exhibit relatively little scatter and are in excellent agreement with the results of Neoh et al.[24] for premixed flames. The present results for diffusion flames yield a collision efficiency of 0.13 with an uncertainty (95% confidence) of 0.03, which is in good agreement with collision efficiencies for OH of 0.13 of Neoh et al.[24] for premixed flames using the same treatment of soot structure as the present investigation.

CONCLUSIONS

Flame structure, primary soot particle surface growth rates, primary soot particle (of TEM-observable particles) nucleation rates, and primary soot particle surface oxidation rates, were studied for laminar jet premixed and diffusion flames involving various hydrocarbon fuels (methane, acetylene, ethylene, propane, propylene, and benzene) for temperatures of 1500-2350 K, and for pressures of 0.1-1.0 atm. These observations have yielded the following major conclusions:

1. Primary soot particle surface growth rates (corrected for effects of soot surface oxidation) in various laminar flame environments agree within experimental uncertainties and are correlated reasonably well by the HACA soot surface growth rate mechanisms of Colket and Hall[18] (after a minor correction to delete their Reaction No. 3 from this mechanism) and Frenklach and coworkers,[19-21] with steric factors in both these mechanisms having values on the order of unity, as expected.

2. Primary soot particle surface (of TEM-observable particles) nucleation rates in various laminar flame environments agree within experimental uncertainties and could be correlated reasonably well by a simplified model, dominated by PAH growth via the HACA mechanism. This approach indicates that rates of primary soot particle (of TEM-observable particles) nucleation exhibit first-order molecular behavior with respect to acetylene and second-order molecular behavior with respect to H.

3. Primary soot particle surface oxidation rates (corrected for effects of soot surface growth) in various laminar diffusion flame environments could be correlated reasonably well by assuming a constant collision efficiency for OH of 0.13 with an uncertainty (95% confidence) of 0.03. This finding is in good agreement with the classical work of Neoh et al.[24,25] based on measurements in laminar premixed flames at atmospheric pressure. The correction of these results for soot surface oxidation by O_2, estimated using the measurements of Nagle and Strickland-Constable,[22] was less than 10%, suggesting that soot oxidation by OH is a dominant feature of the soot-containing flames considered during the present investigation.

These results should provide a way to estimate soot properties in flames. Additional study of primary soot particle surface reaction and nucleation properties is needed, however, in order to resolve effects of pressures greater than atmospheric pressure and effects of hydrocarbons, particularly aromatic hydrocarbons and PAH, other than those considered here. Finally, late soot oxidation, after 70% of the maximum mass of the primary soot particles has been oxidized, when the particles become porous and internal particle oxidation becomes a factor, also merits consideration in order to develop a robust way to estimate soot properties in flames.

ACKNOWLEDGEMENTS

This research was sponsored by NASA Grant Nos. NCC3-661, NAG3-1878, NAG3-2048 and NAG3-2404 under the technical management of D.L. Urban and Z.-G. Yuan of the NASA Glenn Research Center.

REFERENCES

[1] Sunderland, P.B., Köylü, Ü.Ö., and Faeth, G.M., "Soot Formation in Weakly Buoyant Acetylene-Fueled Laminar Jet Diffusion Flames Burning in Air," *Combustion and Flame*, Vol. 100, Nos. 1/2, 1995, pp. 310-322.

[2] Lin, K.-C., Sunderland, P.B., and Faeth, G.M., "Soot Nucleation and Growth in Acetylene/Air Laminar Coflowing Jet Diffusion Flames," *Combustion and Flame*, Vol. 104, No. 3, 1996, pp. 369-375.

[3] Sunderland, P.B., and Faeth, G.M., "Soot Formation in Hydrocarbon/Air Laminar Jet Diffusion Flames," *Combustion and Flame*, Vol. 105, Nos. 1/2, 1996, pp. 132-146.

[4] Xu, F., Sunderland, P.B., and Faeth, G.M., "Soot Formation in Laminar Premixed Ethane/Air Flames at Atmospheric Pressure," *Combustion and Flame*, Vol. 108, No. 4, 1997, pp. 471-493.

[5] Xu, F., Lin, K.-C., and Faeth, G.M., "Soot Formation in Laminar Premixed Methane/Oxygen Flames at Atmospheric Pressure," *Combustion and Flame*, Vol. 115, Nos. 1/2, 1998, pp. 195-209.

[6] Xu, F., and Faeth, G.M., "Structure of the Soot Growth Region of Laminar Premixed Methane/Oxygen Flames," *Combustion and Flame*, Vol. 121, No. 4, 2000, pp. 640-650.

[7] Xu, F., and Faeth, G.M., "Soot Formation in Laminar Acetylene/Air Diffusion Flames at Atmospheric Pressure," *Combustion and Flame*, Vol. 125, No. 1/2, 2001, pp. 804-819.

[8]El-Leathy, A.M., Xu, F., Kim, C.H., and Faeth, G.M., "Soot Surface Growth in Laminar Hydrocarbon/Air Diffusion Flames," *AIAA Journal*, Vol. 41, No. 5, 2003, pp. 856-865.

[9]Xu, F., El-Leathy, A.M., Kim, C.-H., and Faeth, G.M., "Soot Surface Oxidation in Hydrocarbon/Air Diffusion Flames at Atmospheric Pressure," *Combustion and Flame*, Vol. 132, No. 1, 2003, pp. 43-57.

[10]Kim, C.H., El-Leathy, A.M., Faeth, G.M., and Xu, F., "Soot Surface Growth and Oxidation in Laminar Diffusion Flames at Pressures of 0.1-1.0 atm," *Combustion and Flame*, in press.

[11] El-Leathy, A.M., Kim., C.H., Faeth, G.M., and Xu, F., "Soot Surface Reactions in High-Temperature Laminar Diffusion Flames," *AIAA Journal*, in press.

[12] Haynes, B. S., and Wagner, H. G., "Soot Formation," *Progress in Energy and Combustion Science*, Vol. 7, No. 4, 1981, pp. 229-273.

[13] Howard, J.B., "Carbon Addition and Oxidation Reactions in Heterogeneous Combustion and Soot Formation," *Proceedings of the Combustion Institute*, Vol. 23, 1990, pp. 1107-1127.

[14] Richter, H., and Howard, J.B., "Formation of Polycyclic Aromatic Hydrocarbons and Their Growth to Soot — A Review of Chemical Reaction Pathways," *Progress in Energy and Combustion Science*, Vol. 26, Nos. 4-6, 2000, pp. 565-608.

[15] Kennedy, I.M., "Models of Soot Formation and Oxidation," *Progress in Energy and Combustion Science*, Vol. 23, No. 2, 1997, pp. 95-132.

[16] Harris, S.J., and Weiner, A.M., "Surface Growth of Soot Particles in Premixed Ethylene/Air Flames," *Combustion Science and Technology*, Vol. 31, Nos. 3 and 4, 1983, pp. 155-167.

[17] Ramer, E.R., Merklin, J.F., Sorensen, C.M., and Taylor, T.W. "Chemical and Optical Probing of Premixed Methane/Oxygen Flames," *Combustion Science and Technology*, Vol. 48, Nos. 5 and 6, 1986, pp. 241-255.

[18] Colket, M.B., and Hall, R.J., "Successes and Uncertainties in Modeling Soot Formation in Laminar Premixed Flames," *Soot Formation in Combustion*, edited by H. Bockhorn, Springer-Verlag, Berlin, 1994, p. 442-470.

[19] Frenklach, M., and Wang, H. "Detailed Modeling of Soot Particle Nucleation and Growth," *Proceedings of the Combustion Institute*, Vol. 23, 1990, pp. 1559-1566.

[20] Frenklach, M., and Wang, H., *Soot Formation in Combustion*, edited by H. Bockhorn, Springer-Verlag, Berlin, 1994, p. 165-192.

[21] Kazakov, A.,Wang, H., and Frenklach, M., "Detailed Modeling of Soot Formation in Laminar Premixed Ethylene Flames at a Pressure of 10 Bar," *Combustion and Flame*, Vol. 100, Nos. 1/2, 1995, pp. 111-120.

[22] Nagle, J., and Strickland-Constable, R.F., "Oxidation of Carbon Between 1000-2000 ˚C," *Proceedings of the Fifth Carbon Conference*, Vol. 1, 1962, pp. 154-164.

[23] Park, C., and Appleton, J.P., "Shock-Tube Measurements of Soot Oxidation Rates," *Combustion and Flame,* Vol. 20, No. 3, 1973, pp. 369-379.

[24] Neoh, K.G., Howard, J.B., and Sarofim, A.F., "Soot Oxidation in Flames," *Particulate Carbon*, edited by D.C. Siegla and B.W. Smith, Plenum Press, New York, 1980, pp. 261-277.

[25] Neoh, K.G., Howard, J.B., and Sarofim, A.F., "Effect of Oxidation on the Physical Structure of Soot," *Proceedings of the Combustion Institute*, Vol. 20, 1984, pp. 951-957.

[26] Garo, A., Lahaye, J., and Prado, G., "Mechanisms of Formation and Destruction of Soot Particles in a Laminar Methane-Air Diffusion Flame," *Proceedings of the Combustion Institute,* Vol. 21, 1986, pp. 1023-1031.

[27] Garo, A., Prado, G., and Lahaye, J., "Chemical Aspects of Soot Particles Oxidation in a Laminar Methane-Air Diffusion Flame," *Combustion and Flame*, Vol. 79, Nos. 3 and 4, 1990, pp. 226-233.

[28] Hardiquert, M., Cessou, A., Stepowski, D., and Coppalle, A., "OH and Soot Concentration Measurements in a High-Temperature Laminar Diffusion Flame," *Combustion and Flame*, Vol. 111, No. 4, 1997, pp. 338-349.

[29] Heckman, F.A., and Harling, D.F., "Progressive Oxidation of Selected Particles of Carbon Black: Further Evidence for a New Microstructure Model," *Rubber Chemical Technology*, Vol. 39, 1966, pp. 1-13.

[30] Wersborg, B.L., Howard, J.B., and Williams, G.C., "Physical Mechanisms in Carbon Formation in Flames," *Proceedings of the Combustion Institute*, Vol. 14, 1972, pp. 929-940.

[31] Lahaye, J., and Prado, G., "Morphology and Internal Structure of Soot and Carbon Blacks," *Particulate Carbon*, edited by D.C. Siegla and G.W. Smith, Plenum Press, New York, 1981, pp. 33-55.

[32] Hess, W.M., and Herd, C.R., "Microstructure, Morphology and General Physical Properties," *Carbon Black*, edited by J.-B. Donoret et al., 2nd edition, Marcel Dekker, New York, 1993, pp. 89-173.

[33] Köylü¸ Ü.Ö., and Faeth, G.M., "Radiative Properties of Flame-Generated Soot," *Journal of Heat Transfer*, Vol. 115, No. 2, 1993, pp. 409-417.

[34] Köylü, Ü.Ö., Faeth, G.M., Farias, T.L. and Carvalho, M.G., "Fractal and Projected Structure Properties of Soot Aggregates," *Combustion and Flame*, Vol. 100, No. 4, 1995, pp. 621-633.

[35] Ishiguro, T., Takatori, Y., and Akihama, K., "Microstructure of Diesel Soot Particles Probed by Electron Microscopy: First Observations of Inner Core and Outer Shell," *Combustion and Flame*, Vol. 108, No. 1/2, 1997, pp. 231-234.

[36] Dobbins, R.A., "The Early Soot Particle Formation in Hydrocarbon Flames," *Physical and Chemical Aspects of Combustion*, edited by F.L. Dryer and R.F. Sawyer, Gordon and Breach, Amsterdam, 1997, pp. 107-133.

[37] Chen, H.X., and Dobbins, R.A., "Crystallogenesis of Particles Formed in Hydrocarbon Combustion," *Combustion Science and Technology*, Vol. 159, 2000, pp. 109-128.

[38] Dobbins, R.A., Govatzidakis, G.J., Lu, W., Schwartzman, A.F., and Fletcher, R.A., "Carbonization Rate of Soot Precursor Particles," *Combustion Science and Technology*, Vol. 121, 1996, pp. 103-121.

[39] Dobbins, R.A., Fletcher, R.A., and Chang, H.-C., "The Evolution of Soot Precursor Particles in a Diffusion Flame," *Combustion and Flame*, Vol. 115, No. 3, 1998, pp. 285-298.

[40] D'Alessio, A., D'Anna, A, Mintutolo, P., Sgro, L.A., and Violi, A., *Proceedings of the Combustion Institute*, Vol. 28, 2000, pp. 2547-2554.

[41] Zhao, B.. Yang, Z., Johnston, M.V. Wang, H., Wexler, A.S., Balthasar, M., and Kraft, M., "Measurement and Numerical Simulation of Soot Particle Size Distribution Functions in a Laminar Premixed Ethylene-Oxygen-Argon Flame," *Combustion and Flame*, Vol. 133, No. 1/2, 2003, pp. 173-188.

[42] Zhao, B.. Yang, Z., Wang, J., Johnston, M.V., and Wang, H., "Analysis of Soot Nanoparticles in a Laminar Premixed Ethylene Flame by Scanning Mobility Particle Sizer," *Aerosol Science and Technology*, Vol. 37, 2003, pp. 611-620.

[43] Roesler, J.F., Martinot, S., McEnally, C.S., Pfefferle, L.D., Delfau, J.-L., Vovelle, C., "Investigating the Role of Methane on the Growth of Aromatic Hydrocarbons and Soot in Fundamental Combustion Processes," *Combustion and Flame*, Vol. 134, No. 3, 2003, pp. 249-260.

[44] Stein, S.E., and Fahr, A., "High-Temperature Stabilities of Hydrocarbons," *Journal of Physical Chemistry*, Vol. 89, 1985, pp. 3714-3725.

[45] Dalzell, W.H., and Sarofim, A.F., "Optical Constants of Soot and Their Application to Heat Flux Calculations," *Journal of Heat Transfer,* Vol. 91, No. 1, 1969, pp. 100-104.

[46] Krishnan, S.S., Lin, K.-C., and Faeth, G.M., "Optical Properties in the Visible of Overfire Soot in Large Buoyant Turbulent Diffusion Flames," *Journal of Heat Transfer*, Vol. 122, No. 3, 2000, pp. 517-524.

[47] Krishnan, S.S., Lin, K.-C., and Faeth, G.M., "Extinction and Scattering Properties of Soot Emitted from Large Buoyant Turbulent Diffusion Flames," *Journal of Heat Transfer*, Vol. 123, No. 2, 2001, pp. 331-339.

[48] Chase, M.W., Jr., Davies, C.A., Downey, J.R., Jr., Frurip, D.J., McDonald, R.R., and Syverud, A.N., *JANAF Thermochemical Tables*, 3rd ed., *Journal of Physical Chemistry Reference Data*, Vol. 14 (Supplement 1) 1986, p. 1211.

[49] Hamins, A., Gordon, A.S., Saito, K., and Seshadri, K., "Acetone Impurity in Acetylene from Tanks," *Combustion Science and Technology*, Vol. 45, Nos. 5 and 6, 1986, pp. 309-310.

[50] Colket, M.B, III, Seery, D.J., and Palmer, H.B., "The Pyrolysis of Acetylene Initiated by Acetone," *Combustion and Flame*, Vol. 75, Nos. 3 and 4, 1989, pp. 343-366.

[51] Colket, M.B, III, Seery, D.J., and Palmer, H.B., "On Impurity Effects in Acetylene Pyrolysis," *Combustion and Flame*, Vol. 84, Nos. 3 and 4, 1991, pp. 434-437.

[52] Tesner, P.A., "Formation of Dispersed Carbon by Thermal Decomposition of Hydrocarbons," *Proceedings of the Combustion Institute*, Vol. 7, 1958, pp. 546-556.

[53] Tesner, P.A., "Dispersed Carbon Formation by Acetylene Self-Combustion," *Proceedings of the Combustion Institute*, Vol. 8, 1960, pp. 627-633.

Table 1. Soot Formation and Oxidation in Laminar Flames Data Base

Source	Fuel	Oxidizer	Pressure (atm)	No. of Flames
Premixed Flames:[a]				
Xu et al.[4]	C_2H_2	Air	1.0	3
Xu et al.[5]	CH_4	O_2	1.0	3
Diffusion Flames:[b]				
Xu and Faeth[7]	C_2H_2-N_2	Air	1.0	3
El-Leathy et al.[8]	C_2H_4	Air	1.0	1
El-Leathy et al.[8]	C_3H_6-N_2	Air	1.0	1
El-Leathy et al.[8]	C_3H_8	Air	1.0	1
El-Leathy et al.[8]	C_2H_2-C_6H_6-N_2	Air	1.0	3
El-Leathy et al.[11]	C_2H_2-Ar	O_2-Ar	1.0	3
Diffusion Flames:[c]				
Kim et al.[10]	C_2H_2-N_2	Air	0.1-1.0	4

[a] Round laminar jet premixed flames having a 60 mm diameter water-cooled flat-flame burner port with a 6 mm wide annular nitrogen coflow.
[b] Round laminar jet diffusion flames having a 34.8 mm inside diameter fuel port and a 60 mm inside diameter outer oxidizer port.
[c] Round laminar jet diffusion flames having a 3.3 mm inside diameter fuel port in an air coflow.

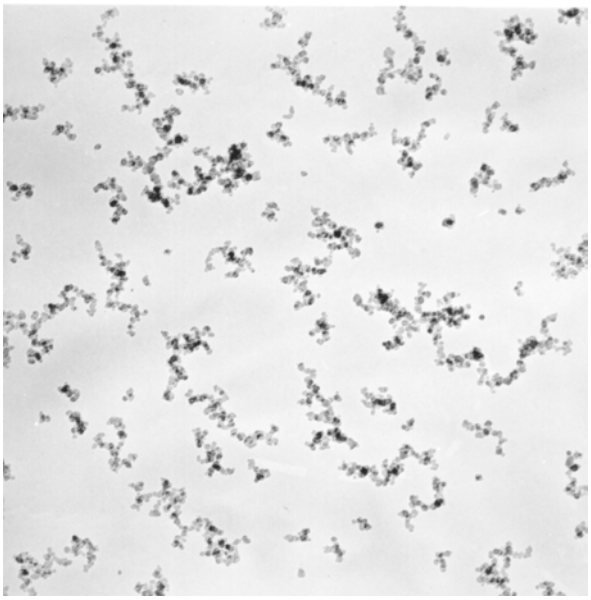

Fig. 1 TEM photograph of soot aggregates along the axis and near the start of the soot formation region of an acetylene-fueled laminar jet diffusion flame burning in an air coflow at 1.0 atm.

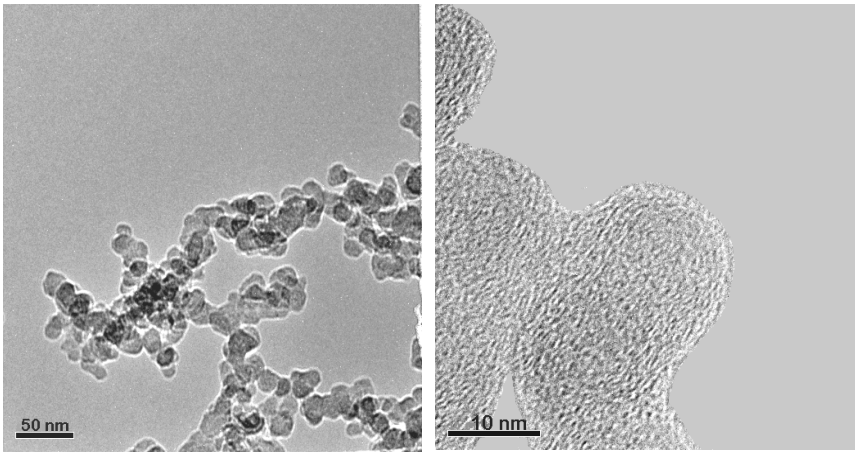

Fig. 2 TEM (left) and HRTEM (right) photographs of soot aggregates along the axis at the end of the soot formation region of an acetylene (12.0% by volume)-argon fueled laminar jet diffusion flame burning in an oxygen (48.18% by volume)-argon coflow at atmospheric pressure.

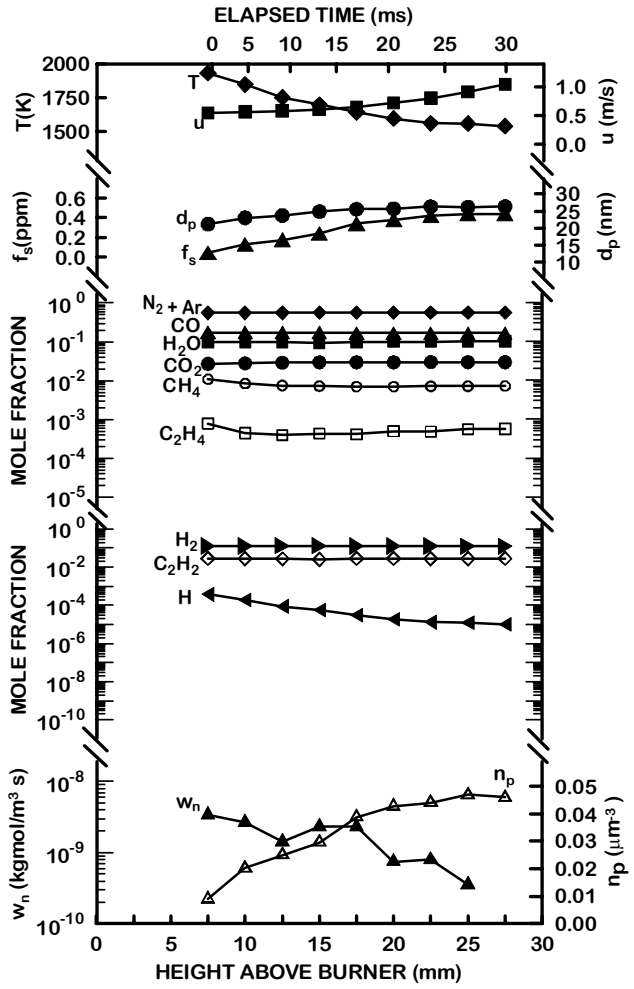

Fig. 3 Measured soot, flame and nucleation properties along the axis of an ethylene (15.6% by volume)-air laminar jet premixed flame at

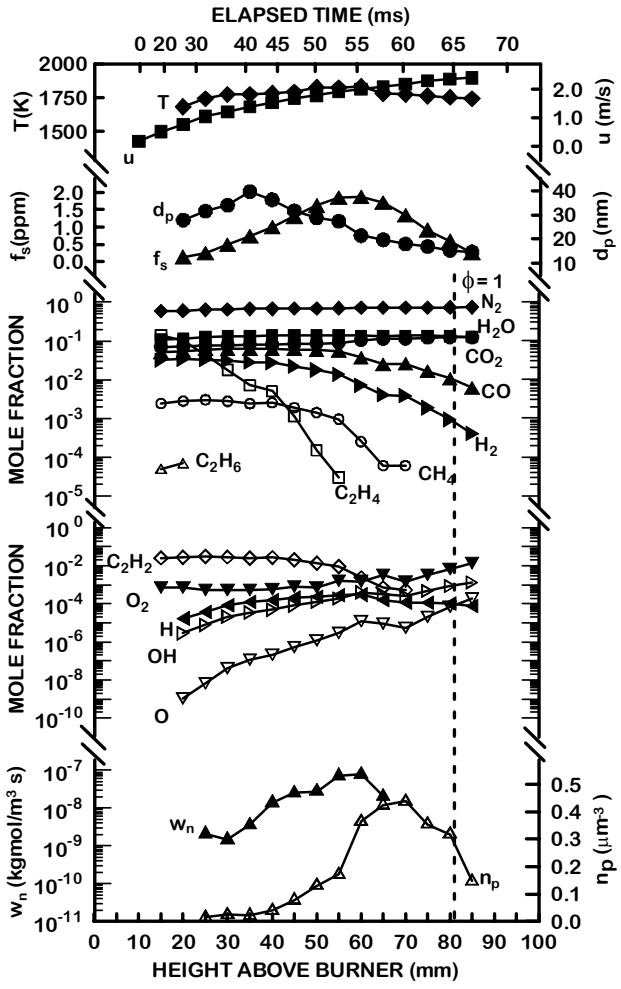

Fig. 4 Measured soot, flame and nucleation properties along the axis of an ethylene-fueled laminar jet diffusion flame burning in air coflow at atmospheric pressure.

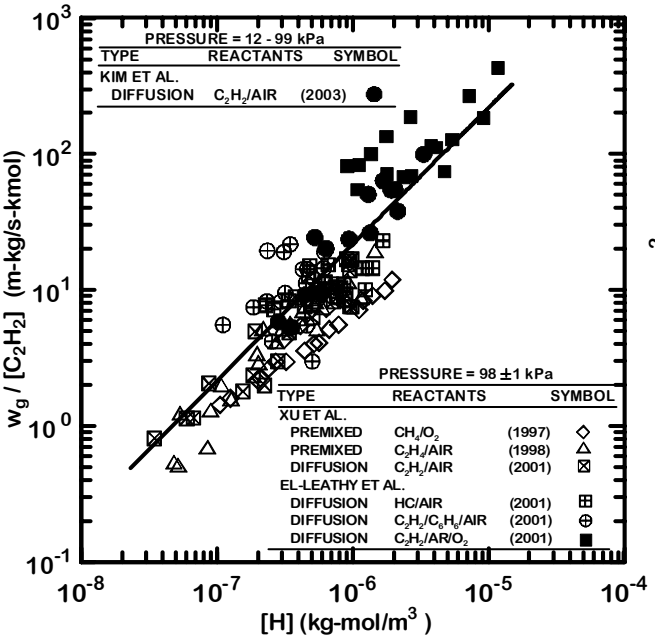

Fig. 5 Soot surface growth rates (corrected for soot surface oxidation) as a function of acetylene and H concentrations for laminar flames at pressures of 0.1-1.0 atm.

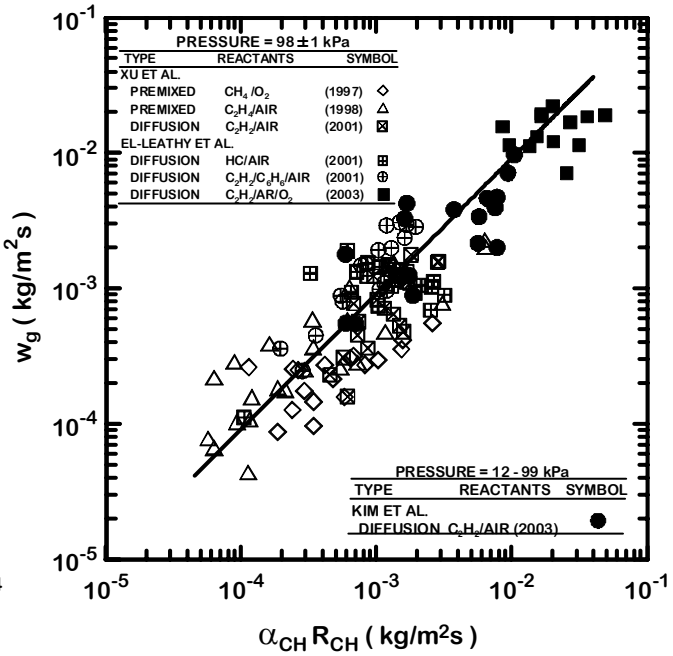

Fig. 6 Soot surface growth rates (corrected for soot surface oxidation) in terms of the HACA mechanism of Colket and Hall[18] for laminar flames at pressures of 0.1-1.0 atm.

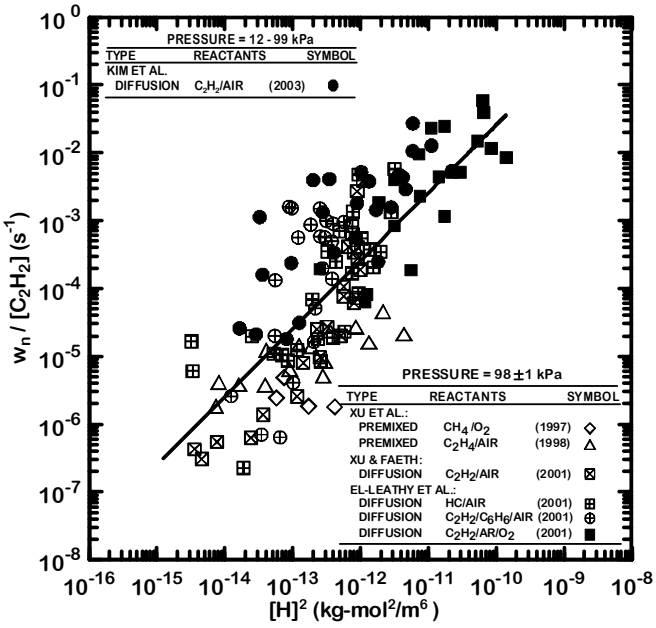

Fig. 7 Soot primary particle nucleation rates as a function of acetylene and H concentrations for laminar flames at pressures of 0.1-1.0 atm.

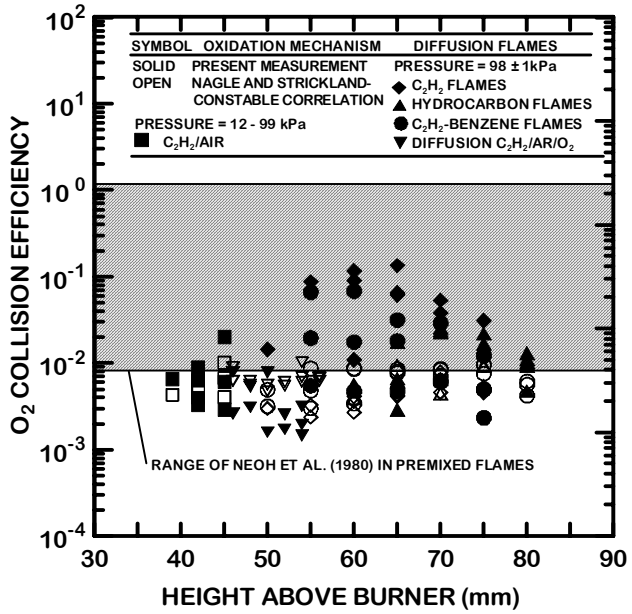

Fig. 8 Collision efficiencies assuming soot surface oxidation (corrected for soot surface growth) due to attack by O_2 as a function of distance from the burner exit for laminar flames at pressures of 0.1-1.0 atm.

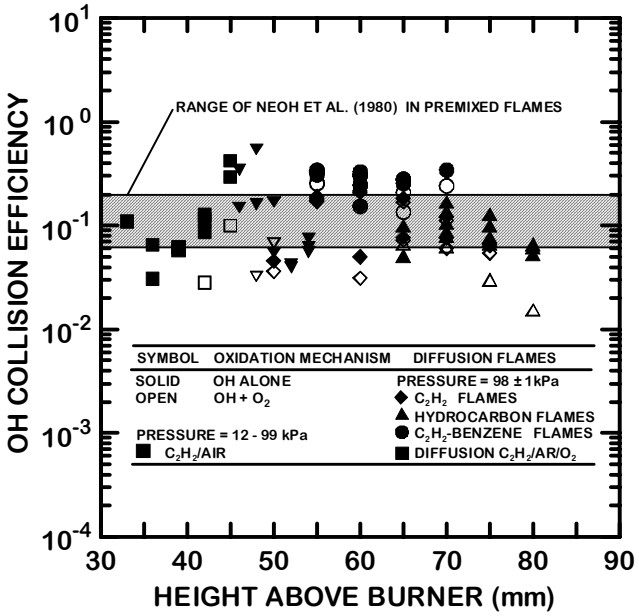

Fig. 9 Collision efficiencies assuming soot surface oxidation (corrected for soot surface growth) due to attack by OH as a function of distance from the burner exit for laminar flames at pressures of 0.1-1.0 atm.